Time-Dependent Mass Spectra and Breakdown Graphs. 21. $C_{14}H_{10}$ Isomers

Yun Ling and Chava Lifshitz*,†

Department of Physical Chemistry and The Farkas Center for Light-Induced Processes, The Hebrew University of Jerusalem, Jerusalem 91904, Israel

Received: September 29, 1997

Unimolecular fragmentations of the anthracene and phenanthrene radical cations $C_{14}H_{10}^{\bullet+}$ were studied by time-resolved photoionization in the vacuum UV, RRKM/QET calculations, and MS/MS with electron ionization. The primary reactions observed are parallel $H^{\bullet}$, H_2, C_2H_2, $C_3H_3^{\bullet}$, and C_4H_2 losses, as well as two consecutive $H^{\bullet}$ losses from $C_{14}H_9^+$ and $C_{12}H_8^{\bullet+}$, respectively. Appearance energies were determined for the microsecond and millisecond time ranges. Activation parameters were deduced for the reactions. The $H^{\bullet}$ and C_2H_2 loss reactions are characterized by loose transition states. The following heats of formation were deduced: ΔH_{f0}° ($C_{14}H_9^+$, anthracenyl) = 282.0 ± 3.0 kcal/mol, ΔH_{f0}°($C_{14}H_9^+$, phenanthrenyl) = 276.4 ± 3.0 kcal/mol and ΔH_{f0}°($C_{12}H_8^{\bullet+}$, biphenylene) ≤ 281.7 ± 3.0 kcal/mol. The C−H bond energies in the anthracene and phenanthrene radical cations are 4.38 ± 0.08 and 3.92 ± 0.10 eV, respectively. The role of isomerization of the parent radical cations prior to dissociation will be discussed.

Introduction

The photostability of polycyclic aromatic hydrocarbons (PAHs) is of importance in view of their astrophysical role.[1] The ionized PAHs are attractive candidates for the diffuse intersteller bands (DIB) which have been known for some time. Noncompact, small linear PAHs such as anthracene were proposed to be responsible for the IR emission.[2] It has been shown[3] that the fragments obtained by irradiation of a PAH cation can be more resistant than the parent PAH ion. Such fragments might be more abundant than PAH cations in the intersteller medium and should be considered in the search for the DIB carriers.

The special resilience of PAHs toward decomposition[4] can be understood: it is due to their high bond energies and their large number of degrees of freedom. These attributes make them attractive candidates for study by time-resolved photoionization mass spectrometry (TPIMS), a technique that we have developed in recent years.[5a] Ions can be trapped in a Paul-type cylindrical ion trap (CIT) for up to several tens of milliseconds.[5b] This allows fragmentations at low energies and enables the determination of "kinetic shifts".[5−9] Owing to the long time scale used, the experiment probes the energy region where fragmentation is in competition with radiative cooling. This is the key region for the study of the survival of PAHs in the intersteller medium.[3a]

We have undertaken a series of detailed studies of the vacuum-UV (VUV) photoionization and fragmentation of naphthalene,[7] phenanthrene,[7] pyrene,[8] and fluoranthene.[9]

In the present study we have concentrated on the anthracene/phenanthrene pair of isomers. The question whether the corresponding radical cations isomerize prior to dissociation remains unsettled. In an earlier experimental study of phenanthrene[7] we have come to the conclusion that acetylene loss forms the most stable $C_{12}H_8^{\bullet+}$ product—acenaphthylene$^{\bullet+}$. Our more recent density functional theory (DFT) calculations,[10] when compared to experimental results to be presented in greater detail here, have shown, based on the energetics of C_2H_2 loss, that the most plausible product is biphenylene$^{\bullet+}$ and that isomerization between anthracene$^{\bullet+}$ and phenanthrene$^{\bullet+}$ may occur prior to acetylene elimination.

A major reaction besides acetylene elimination is C−H bond cleavage. An outcome of our previous studies has been the emergence of a trend in C−H bond energies in ionic PAHs, namely, a rise with increasing PAH size to a limiting value equal to the C−H bond energy in neutral PAHs. As part of the study of the thermochemistry of the ensuing ions, we determined[11] the heat of formation of the anthracenyl cation $C_{14}H_9^+$ and the C−H bond energy in anthracene$^{\bullet+}$ by a VUV photoionization study of C−Br cleavage of 9-bromoanthracene. We found that the C−H bond weakening upon ionization is negligible for anthracene[11] and that the C−H bond energy in anthracene$^{\bullet+}$ is higher than for naphthalene$^{\bullet+}$. On the other hand, our earlier study of phenanthrene[7] has shown that its ion has a lower C−H bond energy than that of naphthalene$^{\bullet+}$.

We have reinvestigated the unimolecular fragmentations of phenanthrene$^{\bullet+}$, and the results will be presented jointly with the ones for anthracene$^{\bullet+}$. We will demonstrate that the C−H bond energy of anthracene cation radical is indeed close to that of the corresponding neutral, while the phenanthrene radical cation has a lower C−H bond energy than its neutral. Microcanonical rate−energy ($k(E)$) dependences will be deduced for the parallel reactions of $C_{14}H_{10}^{\bullet+}$ isomers, and the possible role of isomerization between anthracene and phenanthrene will be discussed.

Experimental Section

The experimental technique of TPIMS has been described in detail recently,[5,7−9] and only a brief description will be given here. Photoionization is induced by a pulsed vacuum-UV light source, either the Hinteregger discharge in hydrogen, producing the many-line spectrum, or the Hopfield continuum in He. Photoions are trapped in a cylindrical ion trap (CIT). They are ejected into a quadrupole mass filter by a draw-out pulse

* To whom correspondence should be addressed.
† Archie and Marjorie Sherman Professor of Chemistry.

S1089-5639(97)03167-8 CCC: $15.00
Published on Web 01/03/1998

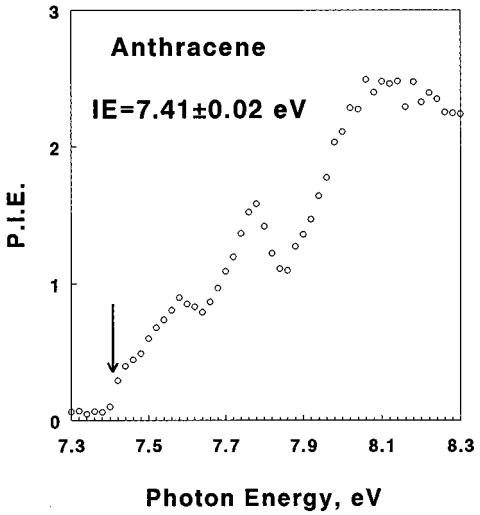

Figure 1. Photoionization efficiency (PIE, arbitrary units) for anthracene parent ion in the threshold-energy range.

following a variable delay time. Ions were stored in this study from 20 μs to 5 ms. The radio frequency (rf) of the potential applied to the cylindrical barrel electrode of the CIT is 0.5 MHz. Ion creation is due to a train of short pulses applied to the light source. An ejection pulse is applied to the end-cap electrode of the CIT nearest the mass filter, and a detection pulse opens the ion counter at the onset of the ejection pulse. The rf voltage is applied to the cylindrical electrode of the CIT throughout the whole cycle. The effective wavelength resolution employed is 5.0 Å. This corresponds to an energy resolution of ~0.025 eV near the ionization threshold of anthracene (7.4 eV) and phenanthrene (7.87 eV) and of ~0.1 eV near the fragmentation onsets.

A simple Knudsen-type molecular-beam source for low-volatility compounds constructed earlier[7] was used to study anthracene and phenanthrene. Effusive beams obtained at temperatures between 353 and 453 K were employed.

High voltage (HV) scans and mass-analyzed ion kinetic-energy spectroscopy (MIKES) studies were carried out on a VG ZAB-2F double-focusing mass spectrometer of reverse geometry.[12]

Anthracene was from Riedel-de Haën (puranal) and SIGMA with a stated purity of 99%. Phenanthrene was from Aldrich with a stated purity of 98%. The samples were used without further purification.

Results and Discussion

Experimental Time-Resolved Photoionization Efficiency Curves. The parent anthracene ion photoionization efficiency (PIE) curve between 7.30 and 8.30 eV is presented in Figure 1. The ionization energy of 7.41 ± 0.02 eV compares favorably with previous determinations 7.40,[13] 7.41 ± 0.02,[14] 7.43,[15] 7.45 ± 0.03,[1] 7.4232 ± 0.0006 eV.[16] Peaks at 7.58 ± 0.02 and 7.78 eV in Figure 1 correspond to the vibrational progression in the photoelectron spectrum.[14] The ionization energy of phenanthrane was measured by us before[7] to be 7.87 ± 0.02 eV.

The photoionization mass spectra obtained for anthracene and phenanthrene at the helium resonance line of 21.21 eV are very similar. The one for phenanthrene is reproduced in Figure 2. The peak due to $CH_3^\bullet$ elimination was too weak for further study. The one due to $(M-2H)^{\bullet+}$ may have contributions from a single step H_2 elimination and/or from two consecutive $H^\bullet$ losses. The energy dependences of the PIEs were studied for

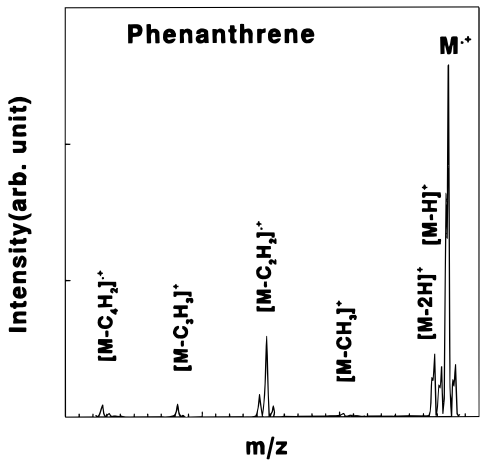

Figure 2. Mass spectrum of phenanthrene at 21.21 eV.

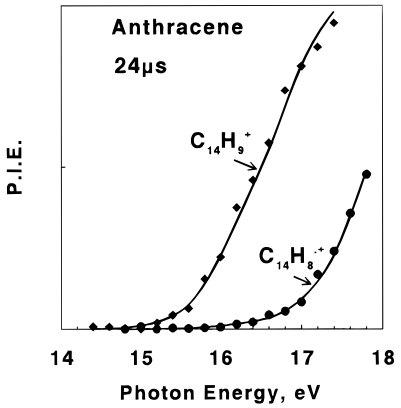

Figure 3. Experimental ((◆) $C_{14}H_9^+$, (●) $C_{14}H_8^{\bullet+}$) and calculated (lines) PIE curves for anthracene in the microsecond range (24 μs).

the following reactions in anthracene$^{\bullet+}$ (I) and phenanthrene$^{\bullet+}$ (II):

$$\rightarrow C_{14}H_8^{\bullet+} + H_2 \quad (1)$$

$$\rightarrow C_{14}H_9^{+} + H^\bullet \quad (2)$$

$$\hookrightarrow C_{14}H_8^{\bullet+} + H^\bullet \quad (3)$$

$$C_{14}H_{10}^{\bullet+} \rightarrow C_{12}H_8^{\bullet+} + C_2H_2 \quad (4)$$

$$\hookrightarrow C_{12}H_7^{+} + H^\bullet \quad (5)$$

$$\rightarrow C_{11}H_7^{+} + C_3H_3^\bullet \quad (6)$$

$$\rightarrow C_{10}H_8^{\bullet+} + C_4H_2 \quad (7)$$

There are four well-established reactions, $H^\bullet$, H_2, C_2H_2, and $C_3H_3^\bullet$ eliminations, that the benzene radical cation undergoes.[17] The two major reactions which naphthalene$^{\bullet+}$ and phenanthrene$^{\bullet+}$ undergo are are $H^\bullet$ and C_2H_2 losses.[7] Additional minor H_2, $C_3H_3^\bullet$, and C_4H_2 eliminations were reported for naphthalene$^{\bullet+}$.[18]

The $C_{14}H_9^+$ and $C_{14}H_8^{\bullet+}$ daughter-ion PIE curves, obtained in the microsecond time range, are presented in Figures 3 and 4 for anthracene and phenanthrene, respectively. Independent MS/MS studies on the ZAB-2F to be described below indicate that the major source of $C_{14}H_8^{\bullet+}$ ions is reaction 3. However, H_2 elimination cannot be ruled out and is at least in part the

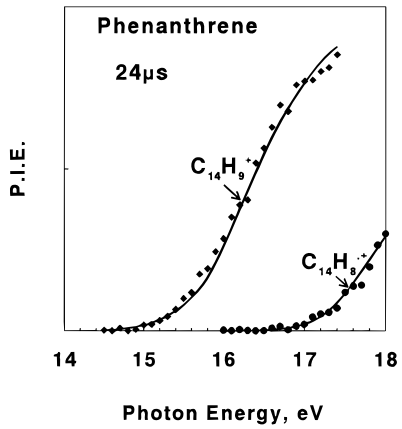

Figure 4. Experimental ((◆) $C_{14}H_9^+$, (●) $C_{14}H_8^{\bullet+}$) and calculated (lines) PIE curves for phenanthrene in the microsecond range (24 μs).

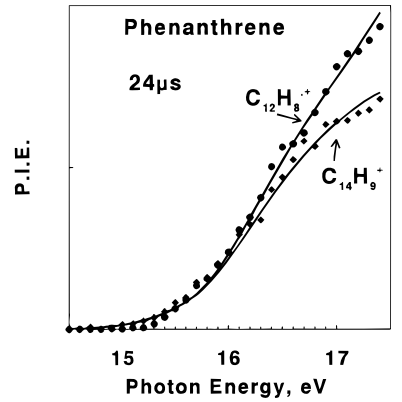

Figure 5. Experimental ((◆) $C_{14}H_9^+$, (●) $C_{12}H_8^{\bullet+}$) and calculated (lines) PIE curves for phenanthrene in the microsecond range (24 μs).

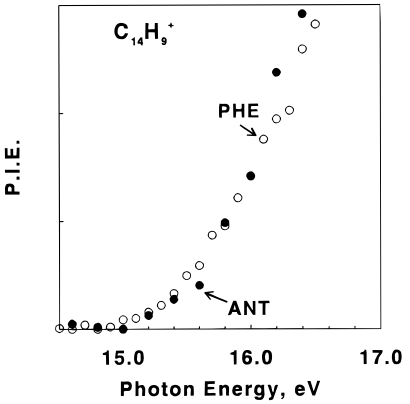

Figure 6. Experimental $C_{14}H_9^+$ PIE curves for anthracene (ANT, ●) and phenanthrene (PHE, ○).

reason for the tailing of the $C_{14}H_8^{\bullet+}$ PIE curve in the case of anthracene (Figure 3), which can be reproduced by RRKM/QET modeling to be described below. The PIE curves for $C_{14}H_9^+$ and $C_{12}H_8^{\bullet+}$ from phenanthrene are nearly superimposable over a range of energies (see Figure 5). The $C_{14}H_9^+$ PIE curves from anthracene and phenanthrene, respectively are nearly superimposable (Figure 6). However, the heat of formation of neutral anthracene,[19] $\Delta H_f°_{298}$ ($C_{14}H_{10}$, ANT) = 55 ± 0.2 kcal is higher than that of phenanthrene,[19] $\Delta H_f°_{298}$ ($C_{14}H_{10}$, PHE) = 49 ± 0.2 kcal/mol. If anthracene$^{\bullet+}$ and phenanthrene$^{\bullet+}$ undergo isomerization to each other below the C−H dissociation limit, one would expect formation of the same (most stable) $C_{14}H_9^+$ isomer from both and one would

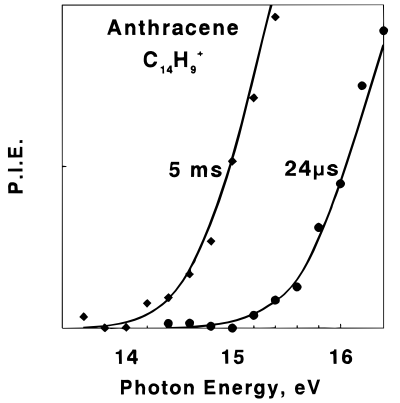

Figure 7. Time-resolved experimental ((●) 24 μs, (◆) 5 ms) and calculated (lines) $C_{14}H_9^+$ (I) daughter-ion PIE curves for anthracene. The PIE curves are in arbitrary units to scale. The relative intensities of the parent served to scale the experimental daughter-ion PIEs.

further expect the $C_{14}H_9^+$ PIE curve from anthracene to be shifted to lower photon energies by 0.26 eV—the difference in the neutral heats of formation. Since this is not the case (Figure 6), we will assume that isomerization does not precede C−H bond cleavage. A similar conclusion can be drawn concerning the $C_{12}H_8^{\bullet+}$ ions: not only is the PIE curve from anthracene not shifted to lower photon energies, it is in fact shifted to energies slightly higher than the one from phenanthrene. Jochims et al.[1] have similarly concluded on the basis of AEs of isomeric ions that the $C_{14}D_{10}^{\bullet+}$ parent ions retain individual structures before fragmentation.

The appearance energies, AEs, of daughter ions were determined from PIE curves with and without trapping. Time-resolved PIE curves for $C_{14}H_9^+$ (I) from anthracene at 24 μs and 5 ms are presented in Figure 7. The relative intensities of the experimental PIE curves of the parent were used to scale the daughter-ion PIEs. Since charge transfer from the daughter ion to the neutral precursor was observed at the long trapping time, the intensities were corrected through measurements at low pressures under which charge transfer was suppressed.

The $C_{14}H_9^+$ (I) daughter-ion PIE curve is observed to shift to lower photon energies with increasing trapping time (Figure 7). Similar shifts were observed for $C_{14}H_8^{\bullet+}$ and $C_{12}H_8^{\bullet+}$ from both anthracene and phenanthrene. The intensities of $C_{11}H_7^+$, $C_{10}H_8^{\bullet+}$, and $C_{12}H_7^+$ were too low for measurements at long trapping times to be made. The shift to lower energies is due to the sampling of lower rate constants with increasing reaction times and has been studied by us in detail before. By ion-trapping, we are able to overcome part of the "conventional" kinetic shift (CS)[6] that is part of the excess energy required to observe detectable (1%) dissociation within ~10 μs. Ion trapping cannot overcome the "intrinsic" kinetic shift (IS),[6] which is the energy needed for 10% fragmentation in competition with radiative relaxation of the excited ion. We have shown[20] that the part due to the IS that cannot be overcome by ion trapping increases with increasing size of the PAH. As a result, the critical energies of activation for reactions 1−7 in anthracene and phenanthrene can only be deduced by a careful modeling analysis of the time-resolved PIE data to be given below.

Time-resolved AEs for daughter ions from anthracene and phenanthrene are presented in Table 1. These values are "vanishing current" values and include therefore contributions from the thermal energy. The average thermal energy in the anthracene experiment was higher (0.49 eV) than in the phenanthrene experiment (0.22 eV). We consider the present

TABLE 1

ion (reaction)	AE, eV (time) anthracene (at 453 K)	phenanthrene (at 353 K)
$C_{14}H_9^+$ (2)	15.0 ± 0.2 (24 μs)	14.9 ± 0.1 (24 μs)
	14.0 ± 0.2 (5 ms)	14.0 ± 0.2 (5 ms)
$C_{14}H_8^{\bullet+}$ (1)	15.8 ± 0.2 (24 μs)	
	15.2 ± 0.4 (5 ms)	
$C_{12}H_8^{\bullet+}$ (4)	15.2 ± 0.2 (24 μs)	15.2 ± 0.1 (24 μs)
	14.2 ± 0.2 (5 ms)	14.1 ± 0.2 (5 ms)
$C_{14}H_8^{\bullet+}$ (3)		16.9 ± 0.3 (24 μs)
		16.0 ± 0.2 (5 ms)
$C_{12}H_7^+$ (5)	17.4 ± 0.2 (24 μs)	17.9 ± 0.2 (24 μs)
	16.4 ± 0.4 (5 ms)	
$C_{11}H_7^+$ (6)	14.8 ± 0.3 (24 μs)	15.5 ± 0.2 (24 μs)
$C_{10}H_8^{\bullet+}$ (7)	15.4 ± 0.2 (24 μs)	15.3 ± 0.2 (24 μs)

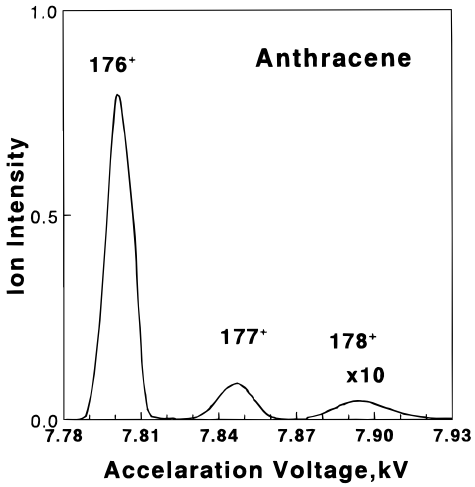

Figure 8. HV scan on the ZAB-2F of *m*/*z* 176 from anthracene. The daughter ion $C_{14}H_8^{\bullet+}$ has two precursors: $C_{14}H_{10}^{\bullet+}$ (I) (*m*/*z* 178) and $C_{14}H_9^+$ (I) (*m*/*z* 177).

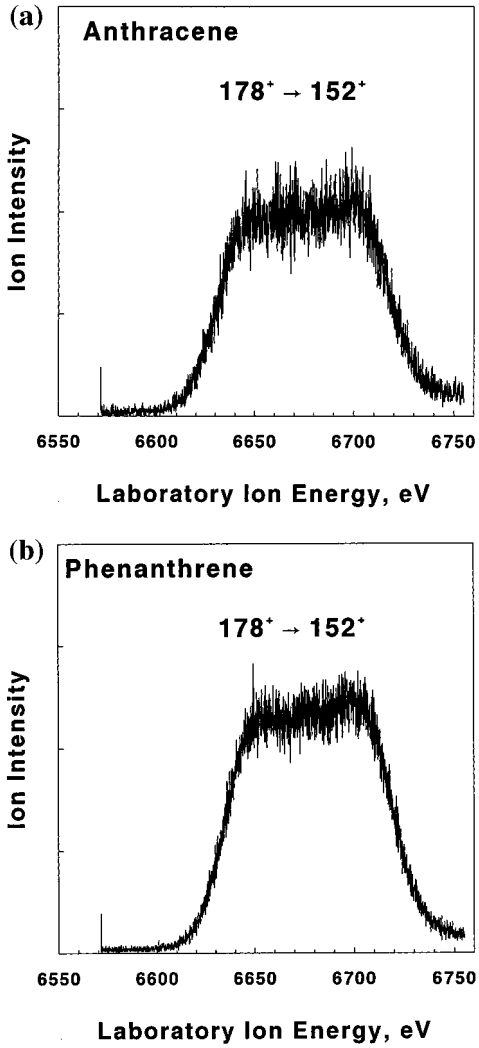

Figure 9. (a) Metastable ion peak shape (second field-free region, ZAB-2F dissociation) for C_2H_2 loss from anthracene. The parent beam had a laboratory energy of 7819 eV. The metastable peak is obtained by scanning the electrostatic energy analyzer (ESA) voltage. (b) Metastable ion peak shape (second field-free region, ZAB-2F dissociation) for C_2H_2 loss from phenanthrene.

data for phenanthrene to be superior to the previous ones[7] owing to higher sensitivity and mass resolution, which allowed the H$^\bullet$-loss measurement for the long trapping time to be made. Our AE values for anthracene are lower than those of Jochims et al.[1] obtained for anthracene-d_{10}. The high AEs reported in the literature[1] for D_2 loss from anthracene-d_{10} and phenanthrene-d_{10} are ascribed by us to two consecutive D$^\bullet$ atom losses. We have reached similar conclusions in the case of pyrene[8] and fluoranthene,[9] namely that AEs assigned to H_2 eliminations are in fact due to two consecutive H$^\bullet$ losses.

The parent-ion PIE curves demonstrate in anthracene as well as in phenanthrene broad resonance peaks due to plasmon excitation, which we have discussed in a separate publication.[21] Although the daughter-ion PIE curves shift to lower energies and increase in relative abundance with increasing trapping time, the parent-ion resonance curves are hardly affected.

MS/MS Spectra. Two types of tandem MS/MS experiments were performed. In high-voltage (HV) scans we mass-selected the daughter ion $C_{14}H_8^{\bullet+}$ or $C_{12}H_7^+$ and obtained spectra of their precursor ions. Figure 8 reproduces the HV scan spectrum for $C_{14}H_8^{\bullet+}$ from anthracene. It demonstrates that in the first field-free region of the ZAB-2F mass spectrometer, in the microsecond time range, $C_{14}H_8^{\bullet+}$ is mainly produced from $C_{14}H_9^+$ (reaction 3). The very low-abundance $C_{14}H_{10}^{\bullet+}$ ion (at m/z = 178) may indicate a low-abundance H_2 elimination (reaction 1), although the occurrence of two consecutive H$^\bullet$ losses in the same field-free region cannot be ruled out. The major contribution to $C_{12}H_7^+$ formation is from $C_{12}H_8^{\bullet+}$ (reaction 5) with a minor contribution from C_2H_2 elimination by $C_{14}H_9^+$.

In MIKES (mass-analyzed ion kinetic-energy spectra), precursor ions were mass-selected by the magnetic field and their product ion peak shapes metastably produced in the second field-free region were determined by scanning the electrostatic analyzer (ESA) voltage. The resultant peak shapes for reaction 4 in anthracene and phenanthrene, part a and b of Figure 9, respectively, are both dish-topped and indistinguishable from one another. The dish-topped nature of the metastable peak shape indicates that the exit channel in the potential-energy profile for acetylene elimination is characterized by a reverse activation energy, which in turn means that the final step in the elimination process is one with a tight transition state. Furthermore, the identity of the peak shapes for the two isomers indicates that isomerization to a common structure, which is the precursor of the final step of the C_2H_2 elimination, does take place.

RRKM/QET Calculations. Time-resolved PIE curves were modeled by RRKM/QET calculations.[7−9] The microcanonical rate coefficients $k(E)$ were calculated as a function of energy

by an RRKM program.[22] The computed vibrational frequencies of anthracene[13] and phenanthrene[10] ions were adopted for the reactant ions. Since the density functional (DFT) calculations,[10] combined with the present modeling, show that the most plausible $C_{12}H_8^{\bullet+}$ isomer formed from C_2H_2 loss of anthracene and phenanthrene is biphenylene$^{\bullet+}$, the vibrational frequencies of $C_{12}H_8^{\bullet+}$ were taken as the computed B3LYP/cc-pVDZ vibrational frequencies of the biphenylene ion. The transition-state vibrational frequencies were varied to get the best agreement with the experimental results. It is widely accepted that the details of the frequency changes in the transition state are not important;[23] the important factor is the degree of tightness or looseness of the transition states, which is characterized by a single parameter—the activation entropy at 1000 K, $\Delta S^{\ddagger}_{1000K}$. The consecutive H$^{\bullet}$ loss from $C_{14}H_9^+$ was treated in a similar manner as before.[9] The internal energy of $C_{14}H_9^+$ was taken as the excess energy above the H$^{\bullet}$ loss critical energy of activation E_0^2. The internal energy of $C_{12}H_8^{\bullet+}$ was calculated under the assumption that the energy available after the dissociation of the $C_{14}H_{10}^{\bullet+}$ precursors is statistically partitioned among the fragments.

In the modeling we have tacitly assumed that anthracene and phenanthrene undergo independent fragmentations without prior isomerization. We will discuss the possibility of assuming isomerization in the modeling later.

Time-resolved parent- and daughter-ion breakdown curves were calculated from the rate-energy k(E) dependences at 0 K. These give the dependences of the fractional abundance of the ions on the internal energy of the parent ion and can be converted into time-resolved curves as a function of photon energy by adding the ionization energy of the molecule to the internal energy of the ion. We have adopted an analytical approach[24] for calculating breakdown curves for consecutive reactions. Resultant breakdown curves for anthracene at t = 24 μs are presented in Figure 10a (parent ion and daughter ions from the major primary and secondary reactions—reactions 2−5) and Figure 10b (daughter ions from minor primary reactions 1, 6, and 7). To distinguish between them, the ion formed by H_2 elimination from the parent is called $C_{14}H_8^{\bullet+}$ (I) while the one formed by consecutive 2H$^{\bullet}$ eliminations is $C_{14}H_8^{\bullet+}$ (II).) The calculated breakdown curves for phenanthrene are very similar to the ones in Figure 10, only slightly shifted to lower photon energies. In addition, a single-step H_2 elimination from phenanthrene$^{\bullet+}$ was not necessary in order to fit the data (see Figure 11). In the calculated breakdown curves (Figures 10 and 11) an additional parallel energy-independent rate process, representing radiative decay and/or collisional cooling, was employed together with the dissociative rates, as was done previously.[7−9] The radiative decay rates that gave best agreement with all experimental PIE curves in this study are 300 s^{-1} for anthracene and 800 s^{-1} for phenanthrene.

The 0-K breakdown curves were convoluted with the instrumental slit function, with the calculated thermal-energy distribution at the temperature of the experiment and with the energy-deposition function. The photoelectron spectra of anthracene[15] and phenanthrene[25] were employed as energy-deposition functions, for anthracene and phenanthrene, respectively. The resultant curves following convolution of the 0-K breakdown curves represent the calculated first derivatives of the PIE curves of the ions, provided the threshold law for photoionization is a step function.[26] These curves are integrated to compare them with the experimental PIE curves. The calculated results are compared with the experimental PIE curves in Figures 3−5 and 7. As in the case of pyrene[8] and fluoranthene,[9] the giant resonance peak in the parent-ion PIE curves could not be fit with the theoretical calculations (Figure 12); however agreement between all experimental and calculated daughter PIE curves was found to be very good.

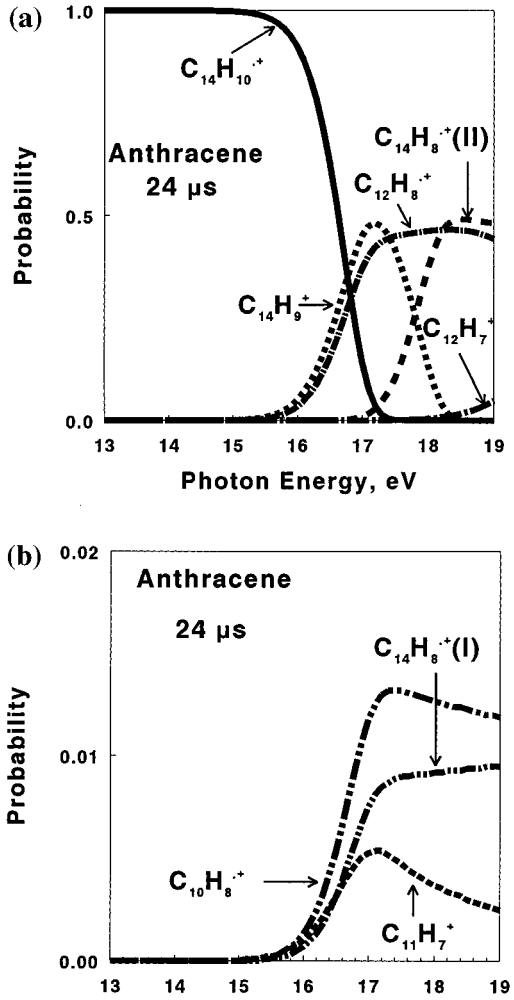

Figure 10. Calculated breakdown curves for anthracene parent and daughter ions at 24 μs.

The activation parameters–the critical energies E_0 and activation entropies $\Delta S^{\ddagger}_{1000K}$–which best fit the whole set of experimental daughter PIE curves of anthracene and phenanthrene are summarized in Table 2, together with σ, which represents the suggested number of equivalent reaction pathways. The uncertainties for the kinetic parameters of consecutive reactions are considerably larger than for the primary reactions. Reactions 2 and 4 in phenanthrene were modeled by us before.[7] The activation parameters deduced for H$^{\bullet}$ loss are quite similar: E_0^2 = 3.92 ± 0.1 eV and $\Delta S^{\ddagger 2}{}_{1000K}$ = 4.4 ± 1 eu (present results) and E_0^2 = 4.1 eV and $\Delta S^{\ddagger 2}{}_{1000K}$ = 4.4 eu (ref 7). However, the ones for C_2H_2 elimination are quite different: E_0^4 = 3.99 ± 0.1 eV and $\Delta S^{\ddagger 4}{}_{1000K}$ = 12.3 ± 1 eu (present results), while E_0^4 = 3.34 eV and $\Delta S^{\ddagger\,4}{}_{1000K}$ = −5.1 eu (ref 7): The previous experimental results were modeled by a much tighter transition state and a lower activation energy for C_2H_2 loss. The tight transition-state model does not fit the present experimental data, which cover all the parallel and consecutive reactions at two ion-trapping times and are considered to be more reliable than the previous data. The large discrepancies between the present and previous activation parameters for acetylene elimination from phenanthrene demonstrate the difficulties encountered due to extrapolation over wide energy ranges. This has been previously demonstrated[7] for naphthalene; two quite extreme

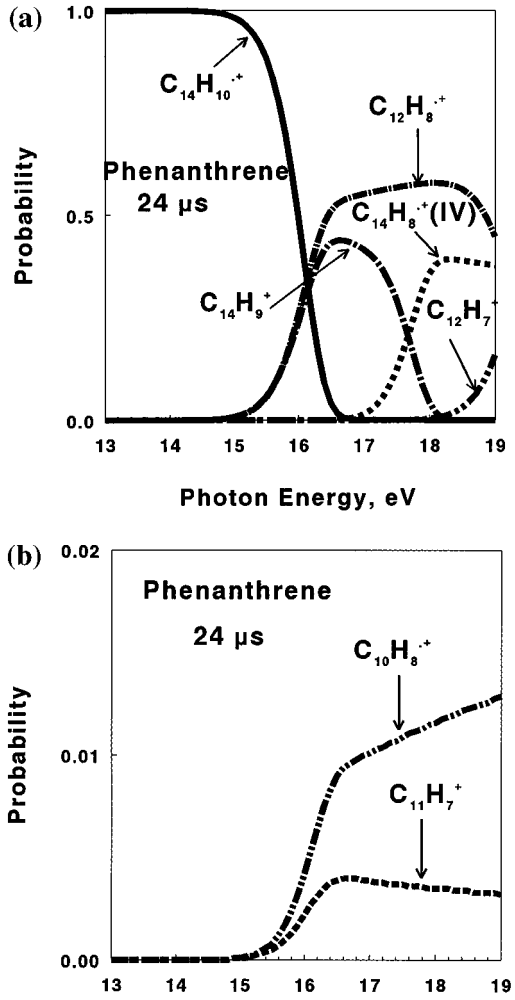

Figure 11. Calculated beakdown curves for phenanthrene parent and daughter ions at 24 μs.

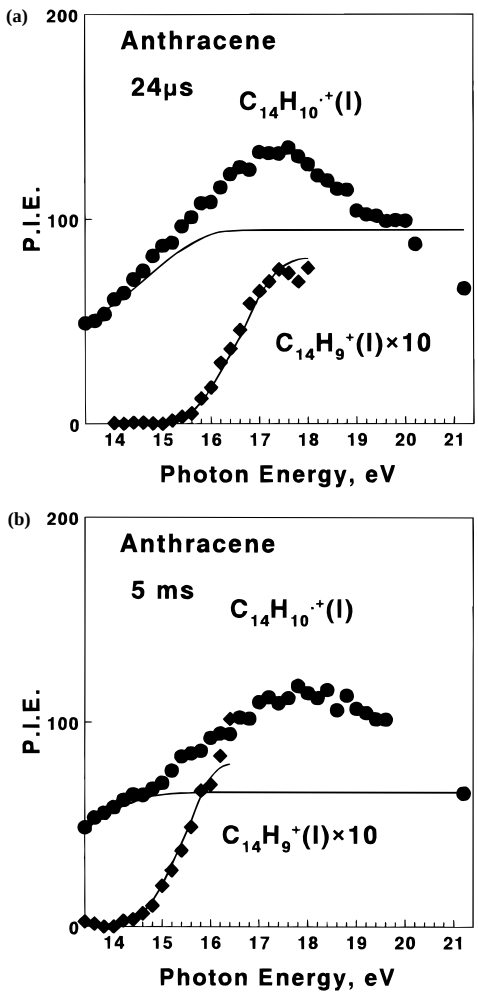

Figure 12. Parent and daughter PIE curves for anthacene [$C_{14}H_{10}^{\bullet+}$ (●, experimental); $C_{14}H_9^+$ (◆, experimental); calculated (lines)] (a) at 24 μs and (b) at 5 ms.

models were able to fit the same set of experimental microcanonical rate constants in the microsecond range. The discrepancies in the case of naphthalene were settled by direct measurements of $k(E)$ in the millisecond range.[27] Direct experimental determinations of $k(E)$ are not available for the $C_{14}H_{10}$ isomers for either the microsecond or the millisecond time ranges. The rate−energy dependences $k(E)$, which best fit the present experimental data, are represented for the major primary reactions, $H^{\bullet}$ loss and C_2H_2 elimination, in Figure 13. The data for phenanthrene and anthracene are plotted together as a function of absolute energy, which is the energy with respect to the constituent elements $14C + 5H_2$ in their standard states at 0 K. It is well-known from the work of Baer and co-workers[28,29] that dissociation rates of isomeric ions are identical at similar absolute internal energies if they rearrange to a common precursor ion prior to dissociation. The $k(E)$ model that fits our experimental results (Figure 13) is not in line with such an interpretation. However, many examples are known in which isomerization and dissociation are in competition.[30,31] Under these conditions the experimentally observed rate constants, k_{obs} are some algebraic combinations of single-step rate constants. The $C_{14}H_{10}^{\bullet+}$ radical cation dissociations follow a multidimensional potential-energy surface, which has not yet been calculated fully by ab initio methods. We have some seemingly contradictory results that may eventually be resolved if a complete ab initio surface will become available. (1) The metastable peak shapes for acetylene eliminations are dish-topped (Figure 9), indicating tight transition states with substantial reverse activation energies; however, the PIE curves were fit by loose transition states (Table 2). (2) The equality of the metastable peak shapes for anthracene and phenanthrene was interpreted as indicating isomerization to a common precursor ion prior to dissociation; however, the $k(E)$ dependences were not found to be equal on the absolute energy scale (Figure 13). The rate constants for anthracene$^{\bullet+}$ are lower than for phenanthrene$^{\bullet+}$ for the same absolute energy. This can be rationalized if there is no fast isomerization between the two, since anthracene$^{\bullet+}$ is 0.21 eV more stable than phenanthrene$^{\bullet+}$ (see coming section) and therefore its density of states is higher. The relatively simple case of a two-well, one-product channel potential-energy surface[30] is characterized by two rate constants. The more stable isomer decomposes by the slower rate constant, while the less stable isomer demonstrates a two-component

TABLE 2: RRKM/QET Parameters

	E_0, eV		$\Delta S^{\ddagger}_{1000K}$, eu		
reaction	ANT[a]	PHE[b]	ANT	PHE	σ
1	4.55 ± 0.2		+2.9 ± 2		2
2	4.38 ± 0.1	3.92 ± 0.1	+5.9 ± 1	+4.4 ± 1	10
3	2.85 ± 0.2	2.91 ± 0.2	−2.0 ± 2	+2.5 ± 2	9
4	4.50 ± 0.1	3.99 ± 0.1	+12.8 ± 1	+12.3 ± 1	1
5	2.95 ± 0.2	3.62 ± 0.2	−14.0 ± 2	+3.1 ± 2	8
6	4.09 ± 0.1	4.05 ± 0.1	−7.9 ± 1	−2.6 ± 1	4
7	4.46 ± 0.1	4.20 ± 0.1	+2.0 ± 1	+4.2 ± 1	2

[a] ANT = anthracene. [b] PHE = phenanthrene.

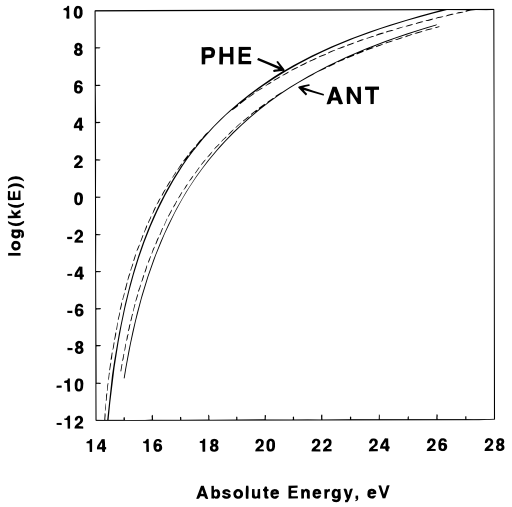

Figure 13. Microcanonical rate constant $k(E)$ (logarithmic scale) as a function of absolute energy (see text): (dashed lines) H• loss; (continuous lines) C_2H_2 elimination; (PHE) phenanthrene; (ANT) anthracene.

decay rate. Our present results indicate (Figure 13) that the isomerization barrier is not very low relative to product formation; otherwise, the two sets of $k(E)$ curves should have coalesced into one (that of the slow rate).

Ion Structures and Thermochemistry. The critical energies of activation E_0 derived from the RRKM modeling (Table 2) can be employed to calculate new bond energies and heats of formation. This has to be done with caution for several reasons. (a) The E_0 values have not been determined directly, and as was noted before, large intrinsic shifts are involved. IS values deduced from the rate−energy dependences are 2.9 eV for H• loss and acetylene elimination from phenanthrene and 3.1 eV for these two reactions in anthracene. (b) The H• loss reactions are characterized by loose transition states, and the critical energies may be equated with the C−H bond dissociation energies of the ions if there are no reverse activation energies. However, the acetylene eliminations are characterized by large kinetic-energy releases, and the activation energies can only give upper limits for the reaction endothermicities. (c) Values deduced for minor primary reaction products such as $C_{11}H_7^+$ and $C_{10}H_8^{\bullet+}$ are less reliable. (d) Critical energies deduced for secondary reactions, such as consecutive H• losses, are even less reliable.

We have equated the critical energies for reaction 2 in anthracene$^{\bullet+}$ and phenanthrene$^{\bullet+}$, 4.38 ± 0.1 and 3.92 ± 0.1 eV respectively, with the corresponding C−H bond energies. The C−H bond dissociation energy in phenanthrene$^{\bullet+}$ is thus considerably lower than in either anthracene$^{\bullet+}$ or in neutral phenanthrene (4.7 ± 0.1 eV).[32] Combining these bond energies with additional thermochemical data (Table 3) allows us to calculate the heats of formation of anthracenyl, $C_{14}H_9^+$(I) and phenanthrenyl, $C_{14}H_9^+$ (II) as follows. The heat of formation of anthracene at 0 K was calculated from the 298-K value[33] and from the anthracene neutral frequencies[13] using standard statistical-mechanics methods: $\Delta H_{f0}°(C_{14}H_{10}) = 62.0$ kcal/mol. Employing the ionization energy gives $\Delta H_{f0}°(C_{14}H_{10}^{\bullet+}$ (I)) = 232.9 kcal/mol. Since $\Delta H_{f0}°(H^\bullet) = 51.63$ kcal/mol, we can calculate the heat of formation of $C_{14}H_9^+$ (I): $\Delta H_{f0}°(C_{14}H_9^+$ (I)) = 282.3 ± 3.0 kcal/mol. This is 6.5 kcal/mol lower than the value obtained from the 9-bromoanthracene study, 288.8 ± 3.0 kcal/mol (ref 11 and Table 3). This difference is very slightly outside the combined estimated error limits and may mean that the average C−H bond energy of the different C−H bonds in anthracene$^{\bullet+}$ is lower than the value for position 9 (Scheme 1). The heat of formation of phenanthrenyl, $\Delta H_{f0}°$-($C_{14}H_9^+$ (II)), was calculated in a fashion similar to that of anthracenyl and found to be 276.4 ± 3.0 kcal/mol.

TABLE 3: Thermochemical Data

species	$\Delta H_{f0}°$,kcal/mol 0 K	298 K	IE, eV
$C_{14}H_{10}$ (anthracene)	62.0[a]	55.44[b]	7.41 ± 0.02[a]
$C_{14}H_{10}$ (phenanthrene)	56.4[a]	49.0[b]	7.86 ± 0.02[d]
$C_{14}H_{10}^{\bullet+}$ (anthracene)	232.9[a]	227[b]	
$C_{14}H_{10}^{\bullet+}$ (phenanthrene)	237.7[d]	230.3[b]	
$C_{14}H_9^+$ (anthracenyl)	282.3 ± 3.0[a]		
	288.8 ± 3.0[c]		
$C_{14}H_9^+$ (phenanthrenyl)	276.4 ± 3.0[a]		
	281 ± 3[d]		
$C_{12}H_8^{\bullet+}$ (I) (biphenylene)	274.7 ± 3.0[a]	279[b]	
$C_{12}H_8^{\bullet+}$ (II) (biphenylene)	268.5 ± 3.0[a]	279[b]	
$C_{12}H_8^{\bullet+}$ (acenaphthylene)	260.2 ± 1[d]	(252)[b]	
$C_{11}H_7^+$ (I) (aceindenyl)	≤245.2 ± 5.0[a]		
$C_{11}H_7^+$ (II) (aceindenyl)	≤249.1 ± 5.0[a]		
$C_{10}H_8^{\bullet+}$ (naphthalene)	229.2[c]	223.6[b]	
C_3H_3• (2-propynyl)		82[b]	
C_4H_2		105[b]	
C_2H_2 (acetylene)	54.7[b]	54.5[b]	
H•	51.63[b]	52.10[b]	

[a] Present results. [b] Reference 33. [c] Reference 11. [d] Reference 7.

SCHEME 1

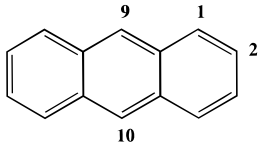

ANTHRACENE $C_{14}H_{10}$

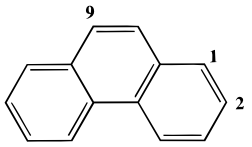

PHENANTHRENE $C_{14}H_{10}$

There are several isomeric $C_{12}H_8^{\bullet+}$ ions that can be formed by acetylene elimination from anthracene$^{\bullet+}$ and phenanthrene$^{\bullet+}$. The question of which isomer(s) is (are) formed has been addressed by us before.[7,10] In our early work on phenanthrene[7] we came to the conclusion that the most stable isomer—acenaphthylene is formed. This agreed with the observation in that paper of a tight transition-state reaction and with the low E_0[4](PHE) = 3.34 eV deduced at the time for reaction 4. Our new experimental results for phenanthrene E_0[4](PHE) = 3.99 eV and for anthracene E_0[4](ANT) = 4.50 eV (Table 2) combined with density functional theory (DFT) calculations led as to the conclusion[10] that both anthracene$^{\bullet+}$ and phenanthrene$^{\bullet+}$ produce biphenylene$^{\bullet+}$. Let us review this decision by comparison with the DFT data and other thermochemical information given in Table 4. Six isomeric $C_{12}H_8^{\bullet+}$ structures have been considered. The calculated dissociation energies of Table 4 do not take into account any reverse activation energies. The minimum reverse activation energy can be estimated to be 6.5−7 kcal/mol (∼0.3 eV) based on the measured minimum KERs, but it can in fact be much higher, as noted earlier, since part of it can end up as internal (vibrational and rotational) energy of the products. If we add 0.3 eV to the thermochemically calculated energy changes for C_2H_2 losses given in Table 4 and compare them

TABLE 4: Dissociation Energies for C_2H_2 Loss or C_4H_2 Loss Predicted from Literature Thermochemistry

	ΔH_{f0}° kcal/mol		$\Delta H_{reaction}$ (0 K) (eV)	
product ion	0 K	298 K	anthracene[d]	phenanthrene[e]
acenaphthylene$^{\bullet+}$	249.5[a]	(252)[b]	3.09	2.88
biphenylene$^{\bullet+}$	274.7[a]	279[b]	4.19	3.98
1-naphthylacetylene$^{\bullet+}$	280.9[a]	(279)[b]	4.45	4.24
2-naphthylacetylene$^{\bullet+}$	282.4[a]	(280)[b]	4.52	4.31
2,3-naphthocyclobutadiene$^{\bullet+}$	283.9[a]		4.59	4.44
1,2-naphthocyclobutadiene$^{\bullet+}$	283.7[a]		4.59	4.44
naphthalene$^{\bullet+}$	229.2[c]	223.6[c]	4.15[f]	3.94[f]

[a] Reference 10. [b] Reference 33 (values in parantheses are less certain). [c] Reference 7. [d] Calculated energy changes for the C_2H_2 or C_4H_2 loss from anthracene radical cation. [e] The calculated energy changes for the C_2H_2 or C_4H_2 loss from phenanthrene radical cation. [f] 298 K value.

with the experimental value for anthracene, we find that only the two most stable isomers, acenaphthylene$^{\bullet+}$ and biphenylene$^{\bullet+}$, are energetically plausible as products from anthracene. Furthermore, if the reverse activation energy is fully converted into kinetic energy of the products, the calculated $E_0 = 4.5$ eV value for biphenylene$^{\bullet+}$ agrees with our experimental value, thus confirming the DFT value ΔH_{f0}°(biphenylene$^{\bullet+}$) = 274.7 kcal/mol. However, if biphenylene$^{\bullet+}$ is also formed from phenanthrene$^{\bullet+}$ and the KER is equated with the reverse activation energy this would require that biphenylene$^{\bullet+}$ be 0.3 eV more stable than the DFT value predicts. Thus, although formation of biphenylene$^{\bullet+}$ at the threshold of C_2H_2 elimination from both isomers is plausible, acenaphthylene$^{\bullet+}$ formation cannot be ruled out. If dissociation were to take place at an internal energy of 4.5 eV (which is not the case because of radiative decay), this would have led in the case of anthracene to the formation of products with as much as 1.1 eV internal energy. It may be the reason behind the seemingly low critical energies required for the consecutive reactions of the $C_{12}H_8^{\bullet+}$ ions, whose modeling did not take into account such high internal energies.

The critical energy for C_2H_2 loss from anthracene$^{\bullet+}$ is only slightly higher than for naphthalene$^{\bullet+}$ (4.50 vs 4.41 eV[27]), and the latter value has been successfully employed[34] to model the photofragmentation of anthracene cations. This lends further support to the present E_0 values and to the thermochemical information deduced for them.

The elimination of C_4H_2 from the $C_{14}H_{10}^{\bullet+}$ isomers leads most probably to naphthalene$^{\bullet+}$. The values for E_0[7] derived from the experiments for 0 K (Table 2) are 4.46 and 4.20 eV for anthracene and phenanthrene, respectively. These are somewhat higher than the thermochemically calculated values for 298 K (Table 4): 4.15 and 3.94 eV, respectively. Elimination of $C_3H_3^\bullet$ leads to the least abundant ion studied, $C_{11}H_7^+$. An upper limit to the heat of formation of $C_{11}H_7^+$ (I) and (II) from anthracene and phenanthrene, respectively, can be estimated by assuming that $C_3H_3^\bullet$ has the linear 2-propynyl, $^\bullet CH_2C{\equiv}CH$ structure. This yields $\Delta H_{f0}^\circ(C_{11}H_7^+, \text{I}) \leq 245.2 \pm 5$ kcal/mol and $\Delta H_{f0}^\circ(C_{11}H_7^+, \text{II}) \leq 249.1 \pm 5$ kcal/mol, which are equal within the error limits. The $C_{11}H_7^+$ ion has probably the stable aceindenyl structure,[35,36] which is aromatic and its formation from anthracene and phenanthrene requires considerable isomerization.

Conclusion

A fairly exhaustive study of the VUV photoionization and fragmentation of the $C_{14}H_{10}$ isomers has been carried out over the energy range ~7−21 eV at two reaction times. This has been combined with RRKM modeling, which led to activation parameters for the major primary and secondary reactions and to heats of formation of some of the key ions. Our data seem to indicate that anthracene$^{\bullet+}$ and phenanthrene$^{\bullet+}$ do not isomerize freely below their dissociation limits but that rather dissociation and isomerization are competing processes. Furthermore, dissociations begin to compete with radiative relaxation of the parent ion only at internal energies in excess of 3 eV above the critical energies for dissociation.

Future studies that can corroborate or refute our findings and deepen our understanding of this complicated system are direct determinations of microcanonical rate constants in the microsecond and/or millisecond regimes and ab initio calculations of the complete multidimensional potential-energy surface.

The conclusions in this study depend rather heavily on the literature values for the heats of formation of the neutral $C_{14}H_{10}$ isomers.[19,33] If the heats of formation of the neutral isomers are nearly equal, then the $k(E)$ curves of Figure 13 would become superimposable and the conclusions concerning interconversion of the isomers below their dissociation limits and concerning the structures of the dissociation products would change.

Acknowledgment. This research was supported by a grant from G.I.F., the German-Israeli Foundation for Scientific Research and Development. The Farkas Research Center is supported by the Minerva Gesellschaft für die Forschung, GmbH, München.

References and Notes

(1) Jochims, H. W.; Rühl, E.; Baumgärtel, H.; Tobita, S.; Leach, S. *Astrophys. J.* **1994**, *420*, 307.
(2) Duley, W. W.; Jones, A. P. *Astrophys. J.* **1990**, *351*, L49.
(3) (a) Boissel, P.; Lefèvre, G.; Thiébot, Ph. Molecules and Grains in Space. AIP *Conf. Proc.* **1994**, *312*, 667. (b) Boissel, P. In *The Diffuse Interstellar Bands*; Tielsens, A. G. G. M., Snow, T. P., Eds.; Kluwer Academic Publishers: Dordrecht, 1994. (c) Granucci, G.; Ellinger, Y.; Boissel, P. *Chem. Phys.* **1995**, *191*, 165.
(4) (a) Pachuta, S. J.; Kenttämaa, H. I.; Sack, T. M.; Cerny, R. L.; Tomer, K. B.; Gross, M. L.; Pachuta, R. R.; Cooks, R. G. *J. Am. Chem. Soc.* **1988**, *110*, 657. (b) Nourse, B. D.; Cox, K. A.; Morand, K. L.; Cooks, R. G. *J. Am. Chem. Soc.* **1992**, *114*, 2010.
(5) (a) Lifshitz, C. *Int. J. Mass Spectrom. Ion Processes* **1991**, *106*, 159. (b) Gotkis, I.; Lifshitz, C. *Org. Mass Spectrom.* **1993**, *28*, 372.
(6) (a) Huang, F.-S.; Dunbar, R. C. *J. Am. Chem. Soc.* **1990**, *112*, 8167. (b) Huang, F.-S.; Dunbar, R. C. *Int. J. Mass. Spectrom. Ion Processes* **1991**, *109*, 151.
(7) Gotkis, Y.; Oleinikova, M.; Naor, M.; Lifshitz, C. *J. Phys. Chem.* **1993**, *97*, 12282.
(8) Ling, Y.; Gotkis, Y.; Lifshitz, C. *Eur. Mass Spectrom.***1995**, *1*, 41.
(9) Ling, Y.; Lifshitz, C. *J. Phys. Chem.* **1995**, *99*, 11074.
(10) Ling, Y.; Martin, J. M. L.; Lifshitz, C. *J. Phys. Chem.* **1997**, *101A*, 219.
(11) Ling, Y.; Martin, J. M. L.; Lifshitz, C. *Int. J. Mass Spectrom. Ion Processes* **1997**, *106*, 39.
(12) Morgan, R. P.; Beynon, J. H.; Bateman, R. H.; Green, B. M. *Int. J. Mass Spectrom. Ion Phys.* **1978**, *68*, 784.
(13) Szczepanski, J.; Vala, M.; Talbi, D.; Parisel, O.; Ellinger, Y. *J. Chem. Phys.* **1993**, *98*, 4494.
(14) Schmidt, W. *J. Chem. Phys.* **1977**, *66*, 828.
(15) Klasinc, L.; Kovac, B.; Güsten, H. *Pure Appl. Chem.* **1983**, *55*, 289.
(16) Cockett, M. C. R.; Kimura, K. *J. Chem. Phys.* **1994**, *100*, 3429.
(17) Kühlewind, H.; Kiermeier, A.; Neusser, H. J. *J. Chem. Phys.* **1986**, *85*, 4427.
(18) (a) Jochims, H. W.; Rasekh, H.; Rühl, E.; Baumgärtel, H.; Leach, S. *Chem. Phys.* **1992**, *168*, 159. (b) Rühl, E.; Price, S. D.; Leach, S. *J. Phys. Chem.* **1989**, *93*, 6312.
(19) Kudchadker, S. A.; Kudchadker, A. P.; Zwolinski, B. J. *J. Chem. Thermodyn.* **1979**, *11*, 1051.
(20) Lifshitz, C. *Int. Rev. Phys. Chem.* **1997**, *16*, 113.
(21) Ling, Y.; Lifshitz, C. *Chem. Phys. Lett.* **1996**, *257*, 587.
(22) Hase, W. L.; Bunker, D. L. *A General RRKM Program*; QCPE No. 234; Chemistry Department, Indiana University; Bloomington, IN.

(23) Lifshitz, C. *Adv. Mass. Spectrom.* **1989**, *11*, 113.
(24) Rodiguin, N. M.; Rodiguina, E. N. *Consecutive Chemical Reactions*; van Nostrand Co.: Princeton, NJ 1964.
(25) Akiyama, I.; Li, K. C.; Le Breton, P. R.; Fu, P. P.; Harvey, R. G. *J. Phys. Chem.* **1979**, *83*, 2997.
(26) Chupka, W. A. *J. Chem. Phys.* **1959**, *30*, 191.
(27) Ho, Y.-P.; Dunbar, R. C.; Lifshitz, C. *J. Am. Chem. Soc.* **1995**, *117*, 6504.
(28) Werner, A. S.; Baer, T. *J. Chem. Phys.* **1975**, *62*, 2900.
(29) Baer, T. *J. Electron Spectrosc. Relat. Phenom.* **1975**, *15*, 225.
(30) Duffy, L. M.; Keister, J. W.; Baer, T. *J. Phys. Chem.* **1995**, *99*, 17862.
(31) Lifshitz, C.; Gotkis, Y.; Ioffe, A.; Laskin, J.; Shaik, S. *Int. J. Mass Spectrom., Ion Processes* **1993**, *125*, R7.
(32) Cioslowski, J.; Liu, G.; Martinov, M.; Piskorz, P.; Moncrieff, D. *J. Am. Chem. Soc.* **1996**, *118*, 5261.
(33) Lias, S. G.; Bartmess, J. E.; Liebman, J. F.; Holmes, J. L.; Levin, R. D.; Mallard, W. G. *J. Phys. Chem. Ref. Data* **1988**, *17* (Suppl. 1).
(34) Boissel, P.; de Parseval, P.; Marty, P.; Lefèvre, G. *J. Chem. Phys.* **1997**, *106*, 4973.
(35) Kurihara, T.; Kerim, A.; Ohta, A. *J. Heterocycl. Chem.* **1994**, *31*, 929.
(36) Brown, R. F. C.; Eastwood, F. W.; Kissler, B. E. *Tetrahedron Lett.* **1988**, *29*, 6861.